Macromolecules

pubs.acs.org/Macromolecules Article

Preferential Control of Forward Reaction Kinetics in Hydrogels Crosslinked with Reversible Conjugate Additions

Thomas M. FitzSimons, Felicia Oentoro, Tej V. Shanbhag, Eric V. Anslyn, and Adrianne M. Rosales*

Cite This: *Macromolecules* 2020, 53, 3738−3746 Read Online

ACCESS | Metrics & More | Article Recommendations | Supporting Information

ABSTRACT: Molecular substitutions were used to demonstrate preferential control over the kinetic rate constants in a poly(ethylene glycol)-based hydrogel with two different reversible thia-conjugate addition reactions. A strong electron-withdrawing nitrile group on the conjugate acceptor showed a 20-fold increase in the forward rate constant over a neutral withdrawing group, whereas the reverse rate constant only increased 6-fold. Rheometry experiments demonstrated that the hydrogel plateau modulus was primarily dictated by reaction equilibrium, whereas the stress relaxation characteristics of the hydrogel were dominated by the reverse rate constant. Furthermore, dynamic crosslinking allowed the hydrogel to rapidly and spontaneously self-heal. These results indicate that decoupling the kinetic rate constants of bond exchange allow systematic control over dynamic covalent hydrogel bulk properties, such as their adaptability, stress relaxation ability, and self-healing properties.

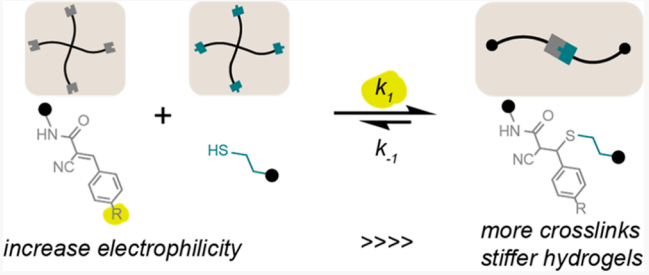

INTRODUCTION

Hydrogels crosslinked with dynamic bonds have shown promising properties for applications such as tissue engineering, drug delivery, and 3-D printing.[1−7] In particular, dynamic bonds confer adaptability to the network, enabling rearrangement on the molecular scale that is dependent on bond lifetime and reaction kinetics.[8,9] This rearrangement can be translated to several useful bulk properties, such as the ability to relax an applied stress or re-form crosslinks across an induced network defect.[10−14] Furthermore, dissociation of dynamic crosslinks may lead to shear-thinning behavior and enhanced injectability.[15−17] For these reasons, engineering bulk hydrogel properties via molecular-level control of dynamic crosslink reactivity has been the subject of intense recent interest.

Dynamic crosslinking chemistries span both noncovalent and covalent bonds. Noncovalent interactions include metal coordination,[18,19] physical entanglement,[20] hydrogen bonds,[21−24] and guest−host complexes.[25] Guest−host complexes in particular have shown a wide range of binding affinities ($K_{eq} \approx 10^2$ to 10^{12} M^{-1})[26] and tunable kinetic parameters for binding that directly translate into a breadth of time-dependent hydrogel mechanics.[27] Dynamic covalent crosslinking, on the other hand, includes a smaller set of explored reactions with slower kinetics,[28] although these are still of intense interest for their robust mechanical properties in polymer networks.[29−32] Despite this recent interest, studies relating systematic variation of bond exchange kinetics to hydrogel properties are limited.

Some dynamic covalent chemistries have been extensively investigated as hydrogel linkages, including hydrazone[8,31,33,34] and boronic ester[4,11,35,36] groups, and emerging reports suggest that control over reaction kinetics can have dramatic and tunable effects on the resulting hydrogel properties.[37,38] For instance, in the case of reversible hydrazone crosslinking, a change from an aliphatic aldehyde to benzaldehyde can significantly slow the forward and reverse rate constants of exchange by 2 orders of magnitude, leading to slower stress relaxation in hydrogels.[33] In another hydrazone crosslinking example, bond exchange kinetics were temporarily accelerated with the use of a benzimidazole-based catalyst, which enhanced hydrogel injectability for cell delivery applications.[39] A third example altered reaction kinetics, and therefore the equilibrium binding constant, using the E/Z isomerization of azobenzene boronic acids to reversibly control hydrogel gel−sol transitions.[40] These reports demonstrate the impact of reversible covalent crosslink kinetics on bulk hydrogel properties and further motivate the preferential control of the forward and reverse rate constants to tailor specific mechanical behavior.

To expand the types of reversible covalent hydrogel linkages, especially with a focus on tunable kinetic parameters, we have explored Michael addition as a dynamic crosslink chemistry. The Michael addition has long been used for efficiently crosslinking hydrogels due to its high yielding "click"

Received: February 10, 2020
Revised: April 26, 2020
Published: May 13, 2020

Downloaded via UNIV OF TEXAS AT AUSTIN on April 20, 2021 at 20:10:32 (UTC).
See https://pubs.acs.org/sharingguidelines for options on how to legitimately share published articles.

© 2020 American Chemical Society

https://dx.doi.org/10.1021/acs.macromol.0c00335
Macromolecules 2020, 53, 3738−3746

nature.[41−45] This reaction consists of a nucleophilic addition to an alkene molecule, such as acrylate, maleimide, or vinyl sulfone. A thiol is commonly used as the nucleophile, and a catalytic amount of base is often added to deprotonate the thiol. Under physiological conditions, this reaction is typically irreversible, but has been shown to be reversible in response to elevated temperature or pH.[46−48] This type of reversible trigger has been used in self-healing vitrimer-type bulk materials, which require a non-physiological trigger to self-heal.[49−52] Recent research has demonstrated, however, that an electron-withdrawing group at the α site of the unsaturated carbonyl introduces reversibility under physiological conditions.[53,54] Subsequent to conjugate addition, deprotonation of the α-carbon, which can be facilitated by the substituent groups on the α carbon, allows the reaction to reverse. This releases a free thiol and recreates the α,β-unsaturated carbonyl by an $E1_{CB}$ mechanism. A small-molecule study investigating this reversible reaction revealed that electron-withdrawing substitutions to an aromatic ring at the β-position could significantly increase the equilibrium constant for the reaction, presumably due to the larger k_1 resulting from enhanced electrophilicity of the reaction site.[55] In this article, we leverage the tunability of the reversible Michael addition kinetics to selectively control hydrogel mechanics.

Toward this goal, we functionalized a multi-arm poly(ethylene-glycol) (PEG) polymer with two distinct conjugate acceptor molecules (Figure 1) and performed kinetic measurements using ultraviolet/visible (UV/vis) spectroscopy with a small molecule thiol to prevent gelation. We demonstrate preferential control over the forward reaction rate kinetics using aromatic substituent group variants, thereby increasing the equilibrium constant while leaving the rate of dissociation relatively unchanged. We then mixed these functionalized PEG macromers with multi-arm thiol-functionalized PEG macromers, which spontaneously gelled in pH 7.4 buffer solution. Because the rate constants dominate different bulk properties, our results show that control of crosslinking kinetics is important for tuning hydrogel plateau modulus independent of stress relaxation. Furthermore, the fast exchange of the reversible Michael addition crosslinks leads to rapid self-healing behavior under physiological conditions, which suggests utility for many hydrogel applications.

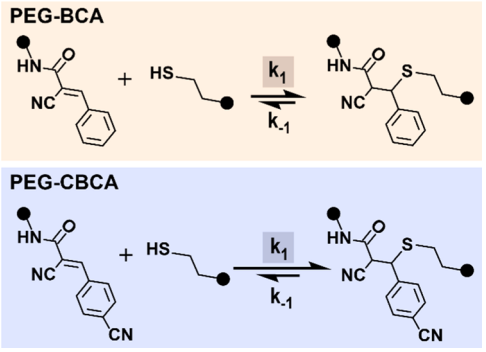

Figure 1. Reaction of an unmodified conjugate acceptor (**PEG-BCA**, in orange) and a *para*-nitrile modified acceptor (**PEG-CBCA**, in blue) with a thiol. Black circles represent either PEG backbone polymers in case of hydrogel formation, or a hydroxyl group in the case of the thiol during UV/vis spectroscopy. Because of the electron-withdrawing strength of the nitrile group, k_1 increases significantly more than k_{-1}. This leads to a shift in equilibrium toward more product formation in the case of **PEG-CBCA**.

EXPERIMENTAL SECTION

Materials. All materials were used as purchased unless otherwise specified. Purchased from Sigma-Aldrich: propargyl amine, anhydrous ethanol, peptide-synthesis grade dimethyl formamide (DMF), phosphate buffered saline (PBS), and dimethyl sulfoxide-d_6 (DMSO-d_6), deuterium oxide, deuterated chloroform, copper sulfate, sodium ascorbate, and β-mercaptoethanol. Purchased from JenKem USA: 4-arm 20k molecular weight PEG-azide and 4-arm 10k molecular weight PEG-thiol. Purchased from Fisher Scientific: methyl cyanoacetate and diethyl ether.

Synthesis of Propargyl Cyanoacetamide (Scheme 1). Propargyl cyanoacetamide was synthesized by adding propargyl amine (5.81 mL, 0.0908 mol, 1.0 equiv) and methyl cyanoacetate (8.01 mL, 0.0908 mol, 1.0 equiv) to an oven-dried round-bottom flask. The reaction proceeded upon stirring for 24 h at room temperature. The product precipitated out and was washed with 200 mL of ice-cold diethyl ether under vacuum filtration. The product was a light yellow solid, yield = 84% (Figure S1). ^{1}H NMR ($CDCl_3$, 400 MHz): δ = 6.28 (s, 1H), δ = 4.1 (dd, 2H), δ = 3.4 (s, 2H), and δ = 2.29 (t, 1H). HRMS (CI): $[M + H]^+$ calcd for $C_6H_7N_2O$, 123.06; found, 123.0558.

Synthesis of PEG-Cyanoacetamide (PEG-CA, Scheme 2). PEG-CA was synthesized via copper-catalyzed click chemistry by adding 4-arm, 20 kDa molecular weight PEG-azide (1 g, 0.05 mmol) and propargyl cyanoacetamide (29.3 mg, 0.24 mmol, 4.8 equiv) to a round bottom flask. This flask was purged with argon for 5 min. Copper(II) sulfate (6.4 mg, 0.04 mmol, 0.8 equiv) and sodium ascorbate (15.8 mg, 0.08 mmol, 1.6 equiv) were added to a separate vial which was also purged with argon. Ultra-filtered water (8 mL) and peptide-synthesis grade DMF (8 mL) were added via syringe to the vial containing copper sulphate and sodium ascorbate. The vial was sonicated to dissolve the solids. This vial was cannulated to the flask containing the PEG and propargyl cyanoacetamide. The mixture was allowed to react for 3 days under constant flow of argon. After 3 days, the contents were precipitated into ice-cold diethyl ether (2 vials with 30 mL ether each). The reaction mixture phase separated into a PEG-containing aqueous layer and an organic layer. The organic layer was discarded, and the aqueous layer was moved to a dialysis bag (6−8 kDa MWCO) and dialyzed against deionized water for 3 days, changing the water every day. After 3 days, the contents were lyophilized. Yield = 99%, functionalization = ∼90% (Figure S2). ^{1}H NMR (DMSO-d_6, 400 MHz): δ = 8.68 (t, 1H), δ = 7.92 (s, 1H), and δ = 3.4 (s, 454H).

Synthesis of Conjugate Acceptor-Functionalized PEG (Scheme 2). A Knoevenagel condensation was used to attach either benzaldehyde or 4-cyanobenzaldehyde to PEG-CA to make **PEG-BCA** or **PEG-CBCA**, respectively. In either case, PEG-CA (272 mg, 0.0136 mmol) and benzaldehyde (552 μL, 5.44 mmol, 400 equiv) or 4-cyanobenzaldehyde (713 mg, 5.44 mmol, 400 equiv) were added to a round bottom flask. The flask was purged with argon. Anhydrous ethanol (5 mL) was added to the flask, which was then heated to 65 °C. The flask was purged with argon for 3 additional minutes. The reaction was allowed to proceed for 2 days. After 2 days, the solution was precipitated into ice-cold diethyl ether (35 mL, three times) to separate the functionalized PEG product from excess aldehyde. After each precipitation, the vial was centrifuged to recover the precipitated solid PEG product, and the supernatant was discarded. After precipitation, the solid product was dried overnight under vacuum. Yield = 99%, functionalization = ∼85% for **PEG-BCA** (Figure S3) and ∼80% for **PEG-CBCA** (Figure S4). ^{1}H NMR (DMSO-d_6, 400 MHz): **PEG-BCA** δ = 8.99 (t, 1H), δ = 8.17 (s, 1H), δ = 7.94 (s, 1H), δ = 7.89 (dd, 2H), δ = 7.51−7.56 (m, 3H), and δ = 3.4 (s, 454H); **PEG-CBCA** δ = 9.11 (t, 1H), δ = 8.25 (s, 1H), δ = 8.04 (d, 2H), δ = 8.04 (d, 2H), δ = 7.96 (s, 1H), and δ = 3.4 (s, 454H).

Rheometry. Rheometry experiments were conducted using a TA Instruments Discovery HR2 rheometer. An 8 mm flat stainless steel

https://dx.doi.org/10.1021/acs.macromol.0c00335
Macromolecules 2020, 53, 3738−3746

geometry on a stainless steel Peltier plate was used for all experiments. Hydrogels were compressed in situ on the rheometer to the appropriate gap height to fill the sample space. The rapid rearrangement of the crosslinks prevented pre-straining the hydrogel. Hydrogels were surrounded with silicon oil after lowering the geometry to the experimental gap height to prevent dehydration. All experiments were done at 25 °C. Amplitude sweeps were performed at 10 rad/s from 0.01 to 2000% strain with an 8 mm stainless steel flat plate geometry. Frequency sweeps were performed from 0.01 to 10 rad/s at 1% strain with a 10 wt % hydrogel and an 8 mm stainless steel flat plate geometry. Stress relaxation experiments used an initial strain of 1% with a 1 s rise time with a 10 wt % hydrogel and an 8 mm stainless steel flat plate geometry. Self-healing high/low strain experiments used 1000 and 0.5% strain, respectively, with a frequency of 10 rad/s and a 10 wt % hydrogel on a 2° stainless steel cone geometry with a diameter of 20 mm.

UV/Vis Spectroscopy. UV/vis measurements were taken on a BioTek Synergy H1 Multi-Mode Microplate Reader. All experiments were done in triplicate at room temperature. The model reaction for all UV/vis measurements was a conjugate acceptor-functionalized 4-arm 20 kDa PEG reacting with β-mercaptoethanol. The extinction coefficient for the reactant conjugate acceptor molecule was determined prior to each experiment, using the Beer−Lambert law and a known concentration and path length. The extinction coefficient for the product was determined by reacting 50 μM of the reactant conjugate acceptor with a >600 times excess of β-mercaptoethanol, which pushed the extent of reaction to 100%. The appropriate amount of excess to ensure complete conversion was determined by recording the concentration of added thiol where the absorbance at the desired wavelength ceased changing (Figures S5 and S6). In the case of these molecules, 150 mM thiol concentration was sufficient for complete conversion of the reactant. The same calculation method as for the reactant conjugate acceptor was used to determine the extinction coefficient (Figures S7 and S8).

Equilibrium constants were determined by measuring the absorbance with relatively equivalent concentrations of conjugate acceptor-functionalized PEG and β-mercaptoethanol in buffer (1× PBS, pH 7.4). By using the Beer−Lambert law for a two-component system, concentrations of the reactant and product were determined (eq S1). These concentrations were used to calculate the equilibrium constant for both **PEG-BCA** and **PEG-CBCA**.

Kinetic rate constants were determined via absorbance on a QE Pro high-performance spectrometer manufactured by Ocean Insight. First, an open top glass cuvette was filled with 1 mL of a 40 μM solution of the conjugate acceptor in PBS (pH 7.4). A small stir bar was added. The absorbance was recorded, and an additional 1 mL of a 40 μM solution of β-mercaptoethanol in PBS was added. This led to an initial concentration for both molecules of 20 μM. Using the same method as for the equilibrium constant, the concentration of all species were determined. The concentration of the conjugate acceptor was plotted versus time and fit to a 2nd order kinetic model that incorporates a 1st order reverse reaction to determine the forward and reverse rate constants (eq S2).

NMR Spectroscopy. ^{1}H NMR spectra (400 MHz) were recorded on an Agilent MR400 spectrometer at room temperature.

Hydrogel Preparation. All hydrogels were formulated at room temperature by mixing **PEG-BCA** or **PEG-CBCA** with a 1:1 stoichiometric amount of thiol-functionalized 4-arm 10 kDa PEG. Unless otherwise stated, the hydrogels contained 10 wt % polymer with functional group concentration around ∼10 mM with variations resulting from slightly different conjugate acceptor functionality. Because of the rapid reaction rates, gelation occurred too rapidly for any vortexing or pipette mixing. The hydrogels were instead mixed manually post-gelation and because of their self-healing behavior were able to rapidly reform into a continuous hydrogel for further experimentation.

RESULTS AND DISCUSSION

Although the reversible Michael addition reaction has been extensively investigated in small molecule systems, few reports examine the utility of this reaction in polymeric networks or hydrogels.[49−52,56−58] In addition, this reaction often requires elevated temperature to induce reversibility. Here, we investigate the impact of controlled rate kinetics on the rheological behavior of PEG hydrogels crosslinked with a dynamic thia-conjugate addition reaction at physiological conditions (Figure 1).

Synthesis and Equilibrium Constant Measurements with a Small Molecule Thiol. To probe the effects of aromatic substituents on the reversible thia-conjugate addition reaction kinetics, we first synthesized two distinct PEG macromers functionalized with benzylcyanoacetamide acceptors: one containing the electron-withdrawing nitrile group in the para position of the aromatic (**PEG-CBCA**) and one without any aromatic substituents (**PEG-BCA**). We developed a progressive synthesis method for PEG functionalization that proceeded via two steps (Scheme 2). In the first step, *N*-propargyl cyanoacetamide (Figure S1) was attached to a 4-arm PEG-azide using copper-catalyzed cycloaddition in water with functionalization of ≥90% (Figure S2). A subsequent Knoevenagel condensation with the substituted benzaldehyde completed the conjugate acceptor. Analysis by ^{1}H NMR spectroscopy indicated high functionalization of the PEG macromer in excess of 80%, as indicated by the emergence of the amine, triazole, and aromatic hydrogens (Figures S3 and S4). Furthermore, the high molecular weight of the PEG conferred water solubility to the conjugate acceptor, allowing subsequent studies to be conducted in buffered aqueous solution.

As a first assessment of the substituent impact on covalent bond formation, we measured the equilibrium constant using a fixed concentration of conjugate acceptor (50 μM) with different amounts of a small molecule thiol, β-mercaptoethanol (Figure 2A). Both the conjugate acceptor and the product

Scheme 1. Synthetic Route for Propargyl Cyanoacetamide

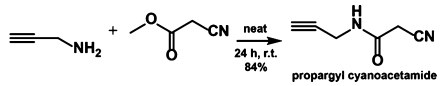

Scheme 2. Synthetic Route for PEG Macromers Functionalized with Conjugate Acceptors

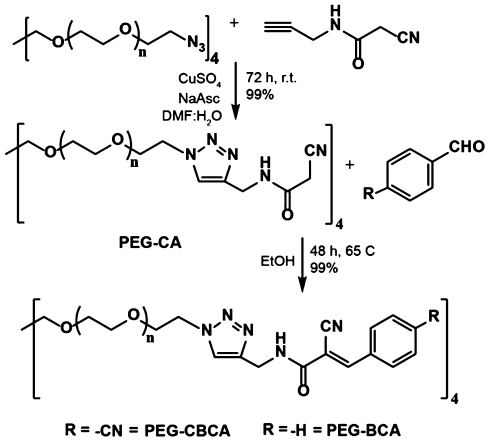

https://dx.doi.org/10.1021/acs.macromol.0c00335
Macromolecules 2020, 53, 3738−3746

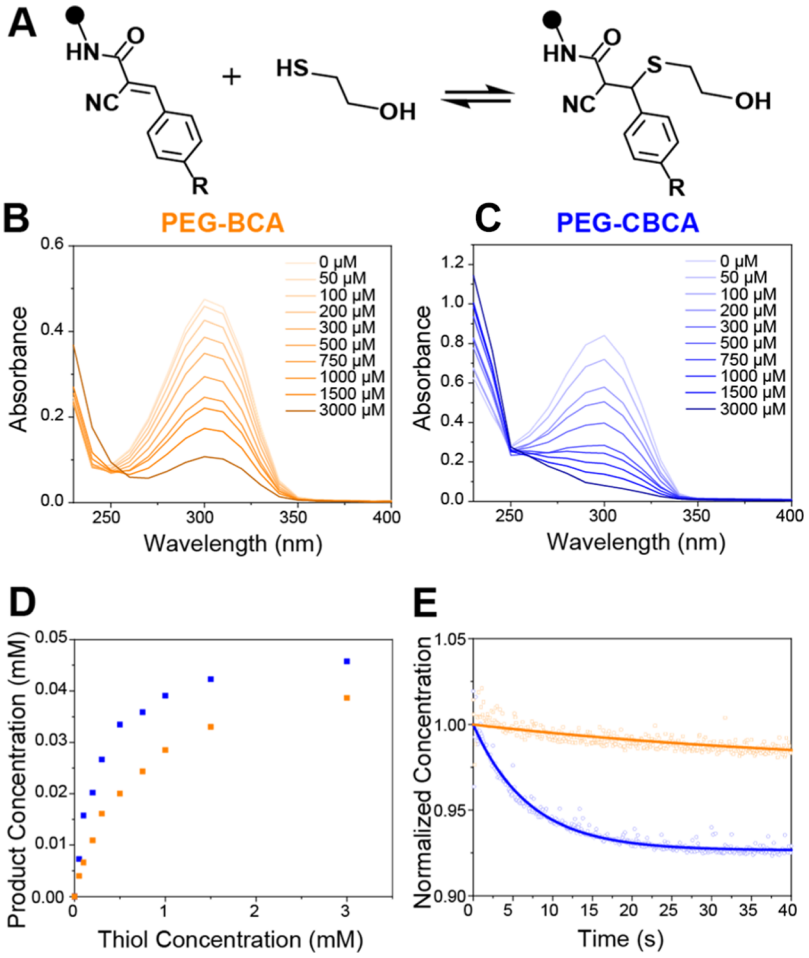

Figure 2. Equilibrium and kinetic studies for both conjugate acceptors. (A) General reaction scheme between the conjugate acceptor and β-mercaptoethanol. (B,C) Absorption spectra of **PEG-BCA** and **PEG-CBCA** with increasing concentrations of thiol. The reactant absorbs strongly at 300 nm, whereas the product does not. (D) Product concentration as a function of thiol concentration for **PEG-BCA** (orange) and **PEG-CBCA** (blue). The maximum for both molecules is 0.05 mM. **PEG-CBCA** reaches this maximum more quickly, demonstrating that it has a larger equilibrium constant. (E) Product concentration for **PEG-BCA** (orange) and **PEG-CBCA** (blue) as a function of time. Fitting the data to a 2nd order kinetic model provides the forward and reverse rate constants.

Table 1. Rate Constants and Equilibrium Constants of Conjugate Acceptors[c]

	k_1 (M^{-1} s^{-1})	k_{-1} (s^{-1})	K_{eq}[a]	K_{eq}[b]	G_∞' (Pa)	crossover (rad/s)
PEG-CBCA	500 ± 50	0.11 ± 0.007	4400 ± 400	4100 ± 600	7500	0.15
PEG-BCA	26 ± 1	0.019 ± 0.0006	1300 ± 60	1200 ± 200	2100	0.09
CBCA/BCA	19.2	5.8	3.4	3.4	3.6	1.7

[a]Time-resolved absorbance measurement. [b]Equilibrium absorbance measurement. [c]All errors are one standard deviation of experiments ran in triplicate.

contain an absorption peak at 300 nm due to the highly conjugated π-bond system. Because the addition of the thiol breaks much of this conjugation, the absorbance at this wavelength for the product is significantly lower than for the reactant. Because of absorption being additive for multiple species, the total absorption is the sum of the conjugate acceptor and product species. The reactant conjugate acceptor extinction coefficient was determined by measuring the 300 nm absorbance of the reactant prior to each experiment. Combining this with our experimentally determined extinction coefficients for the product (Figures S5−S8), we calculated the concentration of all species using the Beer−Lambert equation (eq S1).

Each conjugate acceptor (50 μM) was mixed with different amounts of thiol (ranging from 50 to 3000 μM), and absorbance spectra were measured after 10 min to ensure that the reaction reached equilibration (Figure 2B,C). As thiol concentration increased, more reactant converted to the product (Figure 2D). Dividing the concentration of products to reactants yielded the equilibrium constant, K_{eq}, for both molecules, which we found to be 4100 ± 600 M^{-1} for **PEG-CBCA** and 1200 ± 200 M^{-1} for **PEG-BCA** (Table 1). A previous study that investigated this reaction with two small molecule reactants found $K_{eq} \approx 2700$ M^{-1} for a para-nitro-substituted acceptor and $K_{eq} \approx 390$ M^{-1} for a non-substituted acceptor.[55] Their experiment involved determining reactant and product concentrations via ^{1}H NMR spectroscopy in a pD

https://dx.doi.org/10.1021/acs.macromol.0c00335
Macromolecules 2020, 53, 3738−3746

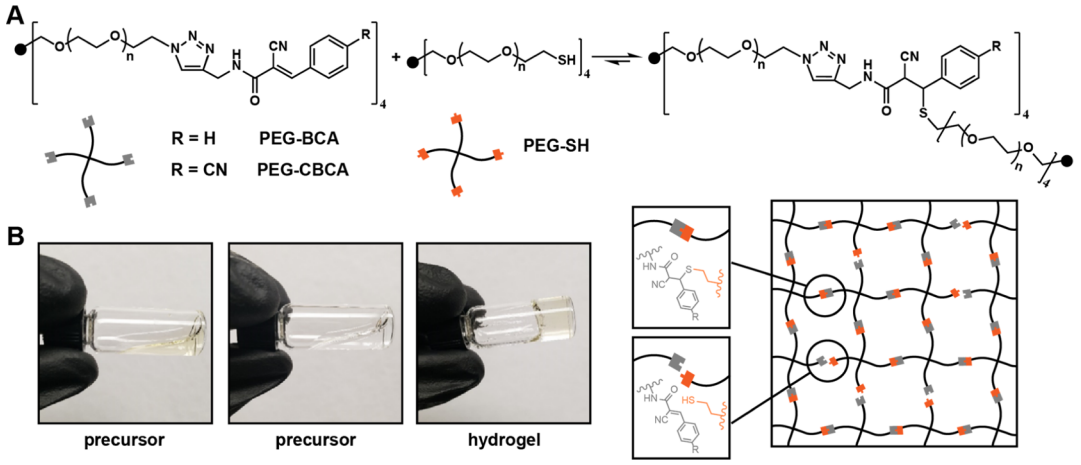

Figure 3. Hydrogel formation using two multi-arm PEG crosslinkers. (A) Reaction between the conjugate acceptor-functionalized PEG and a 4-arm PEG-thiol. The substitution of the small molecule thiol for a multi-arm thiol creates a network when reacted. (B) Mixing the two precursor polymer solutions together creates a hydrogel. A cartoon schematic of an idealized network with the bonds in either a crosslinked or a non-crosslinked state demonstrates the dynamic network.

7.0 buffered solution of CD_3CN/D_2O (5:6). Because water is expected to solvate the thiol of β-mercaptoethanol and there is no thiol in the product, different aqueous solvent systems would presumably affect any measured equilibrium values. Nitro groups are also more strongly electron withdrawing than a nitrile group, and our experiment held the pH constant at 7.4, which should increase kinetic rates. Given these three considerations, there is reasonable agreement between prior studies and this work.

It should also be noted that at longer time scales the acceptor hydrolyzed along the double bond at the reactive site in a reversal of the Knoevenagel condensation reaction that adds the aromatic aldehyde. The **PEG-CBCA** hydrolyzed considerably faster than **PEG-BCA** (approximately 4 times faster, Figures S9 and S10), and the addition of a thiol that can compete with this hydrolysis significantly reduced the rate of hydrolysis by factors of 3 and 4 in the case of **PEG-CBCA** or **PEG-BCA**, respectively (Figures S11 and S12). For **PEG-CBCA** conjugated to a thiol in pH 7.4 buffer, this translated to a stability half-life of 1.9 days. Interestingly, the half-life for conjugated **PEG-BCA** in pH 7.4 buffer was 12.7 days, a 6.6-fold difference. Thus, the molecular structure dictates bulk hydrogel stability and may influence the suitability of these hydrogels for particular applications (e.g., injectable release systems vs longer term use). The tunability of this system may also allow other functional group incorporation to increase the stability of the hydrogel to hydrolysis past that of the **PEG-BCA** polymer. For example, an electron-donating group on the aromatic ring may theoretically increase the hydrolysis half-life. For the purposes of this study, we focused on bulk studies at much lower timescales to ensure that our hydrogel measurements were not significantly impacted by hydrolysis.

Kinetic Studies with β-Mercaptoethanol. The increase in K_{eq} for **PEG-CBCA** compared to **PEG-BCA** indicated that k_1 was accelerated due to the nitrile substituent. We therefore determined the kinetic parameters by monitoring the decrease in conjugate acceptor absorbance upon introduction of β-mercaptoethanol over time and fitting these data to a 2nd order kinetic model that incorporates a 1st order reverse reaction (eq S2). Similar to the equilibrium experiment discussed above, the formation of the thiol−ene bond breaks the conjugation of the acceptor, shifting the maximum absorbance of the product further away from 300 nm. Indeed, the absorbance of the **PEG-CBCA** decreased faster than that of the **PEG-BCA** upon addition of an equimolar amount of β-mercaptoethanol (Figure 2E). Because of the strong absorption of the reactants, we used low concentrations (20 μM) to stay within the UV/vis detector range, which in turn yielded low conversions. However, we were still able to quantify the kinetic rate constants by calculating concentration via the Beer−Lambert law and fitting to a two-component addition reaction model (eq S2) with the forward and reverse reaction rate constants as the fitting parameters (Table 1).

The addition of an electron-withdrawing nitrile group on **PEG-CBCA** led to a 19-fold increase in k_1 as compared to that of **PEG-BCA**: 500 ± 50 and 26 ± 1 mol L^{-1} s^{-1}, respectively. In contrast, the reverse reaction rate constant k_{-1} only increased by approximately 6-fold: 0.11 ± 0.007 s^{-1} for **PEG-CBCA** and 0.019 ± 0.0006 s^{-1} for **PEG-BCA**. A significant increase in k_1 likely results from the increased electron-withdrawing strength of the aromatic substituent, which enhances the electrophilicity of the reaction site on the conjugate acceptor. Less expected was the increase in k_{-1} for **PEG-CBCA**; however, the reaction mechanism sheds insight to this observed result (Figure S13). In the reverse mechanism for this reaction, the α carbon must be deprotonated. The substituent groups at the α site more strongly influence this deprotonation, but changes to the β site may still slightly affect the ability for the α carbon to deprotonate. The inclusion of the strong electron-withdrawing group to the β site aromatic ring may help stabilize the deprotonated α site. The equilibrium constants calculated from these data were in excellent agreement with those provided by the equilibrium absorbance measurements. Overall, these results indicated the ability to preferentially tune k_1 with a substituent in the para position of the benzylcyanoacetamide.

Gelation and Mechanical Characterization of Hydrogels. We next sought to investigate the impact of tuning the kinetic parameters on the bulk properties of hydrogels crosslinked with this reversible thia-benzylcyanoacetamide conjugate addition. To form hydrogels, 4-arm 20 kDa **PEG-BCA** or **PEG-CBCA** was mixed with a stoichiometric amount of 4-arm 10 kDa PEG-thiol in PBS (pH 7.4) (Figure 3A). Gelation occurred within seconds and was too rapid to

https://dx.doi.org/10.1021/acs.macromol.0c00335
Macromolecules 2020, 53, 3738−3746

determine gelation times via shear oscillatory rheometry (Figure 3B). To ensure proper mixing, the hydrogels were prepared by pipetting a solution of PEG-thiol into a solution of the conjugate acceptor-functionalized PEG, and the hydrogels were mixed post-gelation gently in situ. Because the crosslinks are dynamic, any defects created during this mixing were eliminated as the hydrogel healed.

To characterize the viscoelastic nature of the hydrogels, both a strain sweep and a frequency sweep were performed on a rheometer. As the strain increased from 0.01 to 2000%, both hydrogels were in the linear viscoelastic regime for strains as low as 0.01% and showed rupturing around 1000% strain (Figure S14). Thus, subsequent frequency sweeps were performed at 1% strain. The frequency sweep measures the shear storage (G') and loss (G'') moduli of the hydrogels at variable frequencies, ranging from 0.01 to 10 rad/s. Because of the dynamic nature of the crosslinks, the network can rearrange and alleviate network stress resulting from the applied shear forces. The frequency of rotation and bond kinetics both influence the measured storage and loss moduli. With a sufficiently low rotational frequency relative to the bond kinetics, the hydrogel can dissipate the majority of any accumulated shear stress, leading to a G'' that is higher than G'. For these low frequencies, the hydrogel acts as a viscous liquid rather than an elastic solid. Both the **PEG-CBCA** and the **PEG-BCA** hydrogels displayed moduli in this terminal regime that scaled with frequency according to the viscoelastic liquid behavior, that is, $G' \approx \omega^2$ and $G'' \approx \omega$ (Figure S15). At high rotational frequencies relative to the bond kinetics, the crosslinks do not have sufficient time to rearrange, and the hydrogel accumulates stress along the polymer chains. This leads to a G' that is higher than G'', wherein the hydrogel acts as an elastic solid. Both the **PEG-CBCA** and **PEG-BCA** hydrogels exhibited this type of viscoelastic behavior (Figure 4A,B).

At sufficiently high frequencies (>1 rad/s), the hydrogels reached the plateau modulus (G_∞'), which is the maximum storage modulus achievable for the network based on the crosslinking density (a function of K_{eq} of the crosslinking reaction). As the polymer concentration was varied from 5 to 10 wt %, the resulting G_∞' also increased for both the **PEG-CBCA** and the **PEG-BCA** hydrogels (Figure S16). For the 10 wt % hydrogels, the **PEG-CBCA** constructs reached a higher G_∞' of 7500 Pa as compared to that of **PEG-BCA** at 2100 Pa (Table 1). As expected, the larger K_{eq} for the CBCA conjugate acceptor led to a higher G_∞', as more crosslinks are present at any given time. Notably, the ratio of G_∞' for the **PEG-CBCA** hydrogel to G_∞' for the **PEG-BCA** hydrogel was 3.6, which is in excellent agreement with the ratio of K_{eq} for **PEG-CBCA** to K_{eq} for **PEG-BCA** (Table 1).

As a control, the **PEG-CBCA** and the **PEG-BCA** hydrogels were also compared to a hydrogel crosslinked with a thiol-acrylate Michael addition linkage that was irreversible at these conditions (Figure S17). Polymer concentration and pH were identical to the reversible hydrogel experiments at 10 wt % and pH 7.4, respectively. Because the dynamic covalent hydrogels are in equilibrium, their G_∞' was lower than that of the irreversible hydrogel, which showed $G_\infty' \approx$ 10,500 Pa. As anticipated, this result indicated lower crosslinking density in both the **PEG-CBCA** and the **PEG-BCA** hydrogels. Using rubber elasticity theory, these crosslinking densities were estimated to be approximately 7 mM for the **PEG-CBCA** hydrogel and 2 mM for the **PEG-BCA** hydrogel, whereas the

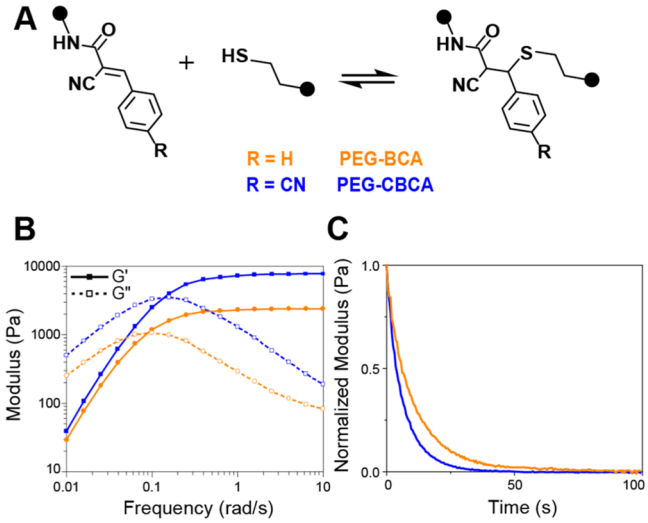

Figure 4. Mechanical testing of both conjugate acceptors. **PEG-BCA** is in orange, and **PEG-CBCA** is in blue. (A) Schematic for the reaction between conjugate acceptor-functionalized PEG and thiol-functionalized PEG. (B) Frequency sweep of both conjugate acceptors. At sufficiently high frequencies (>1 rad/s), both networks behave as elastic solids, but **PEG-CBCA** shows a higher plateau modulus as a result of its larger equilibrium coefficient. The crossover point between G' and G'' for both molecules is around the same mark (~0.1 rad/s). (C) Normalized stress relaxation of both molecules through time. When fit to an exponential decay model, the stress relaxation time constant for **PEG-BCA** was 10.8 s, and the stress relaxation time constant for **PEG-CBCA** was 6.4 s.

irreversible thiol-acrylate hydrogel had a crosslinking density of 9.8 mM. For both the thiol-acrylate hydrogel and the **PEG-CBCA** hydrogel, these values compared favorably to the predicted crosslinking density using K_{eq} and the probability that each macromer has 3 or 4 arms crosslinked to yield elastically active chains in the network (Table S1).[59] The **PEG-BCA** hydrogel, however, showed larger deviation between the calculated and predicted values for the crosslinking density.

The frequency sweep also provided insight to the bulk relaxation behavior of the hydrogel at the crossover point of G' and G'' (Figure 4B). The crossover point can be used as a marker for transition from a viscous liquid to an elastic solid. The faster rate kinetics for the **PEG-CBCA** hydrogels led to a slightly larger crossover point, 0.15 rad/s, compared to 0.09 rad/s for the **PEG-BCA** hydrogels. Compared to the larger difference in G_∞', the crossover points for the two hydrogels were more similar (~1.7 fold difference) (Table 1).

To further probe the similarity in relaxation behavior, a stress relaxation test was performed. During this experiment, the instrument rotated to a fixed strain and measured the shear stress over time. Because of the dynamic crosslinking in these hydrogels, the stress spontaneously dissipated (Figure 4C). By fitting an exponential decay model to the data (eq S4), a stress relaxation time constant, τ, was determined (Figure S18). In agreement with the crossover point data from the frequency sweep experiment, the **PEG-CBCA** hydrogels had a slightly faster τ (6.4 s) than the **PEG-BCA** hydrogels (10.8 s) by a factor of approximately 1.7 (Table S2). The theoretical stress relaxation time, τ, has been previously related to k_{-1} in covalent adaptable networks using a direct inverse proportionality ($\tau = 1/k_{-1}$).[60] Although the **PEG-CBCA** hydrogel showed good agreement between the measured and predicted

https://dx.doi.org/10.1021/acs.macromol.0c00335
Macromolecules 2020, 53, 3738−3746

values of τ, the **PEG-BCA** hydrogel again showed larger deviation (Table S2). Ongoing studies are further investigating the cause of this deviation. Overall, however, we note that the relaxation time scales for both the **PEG-CBCA** and the **PEG-BCA** hydrogels were of the same order of magnitude, which is in contrast to other reversible covalent crosslinking chemistries where molecular changes can lead to a difference in relaxation times from seconds to hours.[33] Taken together, these data show the ability to control G_∞' while maintaining similar stress relaxation, a property that may be useful in applications such as biomaterials.

Self-Healing. Because of the continuous rearrangement of bonds, the synthesized hydrogels demonstrated self-healing behavior, where defects or cuts repair upon contact. Bonds on one side of the defect can separate and re-form across the defect. Because the exchange kinetics for this thia-conjugate addition reaction are rapid, complete self-healing for this material occurred on the order of minutes (Figure 5A). Two

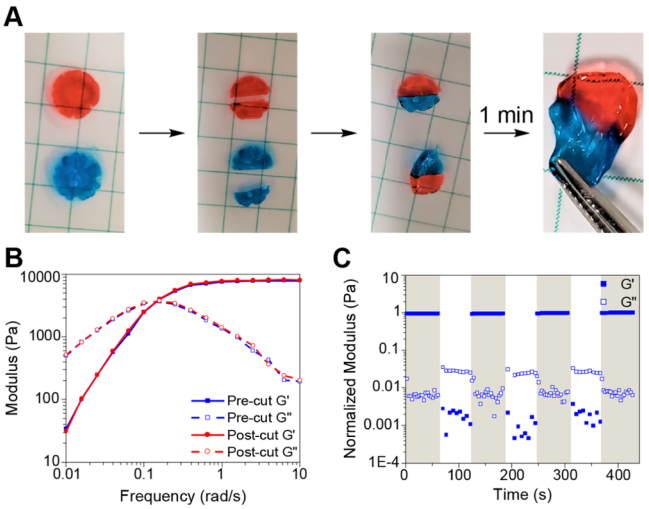

Figure 5. Self-healing behavior of the **PEG-CBCA** hydrogels. (A) Two hydrogels made with the **PEG-CBCA** molecule were dyed with red and blue food coloring. Each was cut in half and then matched to an opposing colored half. After one minute, the hydrogel healed the cut, and was able to be pulled without tearing. (B) Frequency sweep of the hydrogels before being cut, and after being self-healed, shows that the mechanical properties are fully recovered. (C) Storage modulus is shown as a function of time in multiple strain regimes. Transitions between high-strain regimes (unshaded, 1000%) and low-strain regimes (shaded, 0.5%) while held at a constant frequency of 10 rad/s demonstrate the self-healing nature of the hydrogel. High strain ruptures the hydrogel leading to a sharp decrease in the storage modulus, whereas the storage modulus is recovered during the low-strain regimes.

hydrogels using the **PEG-CBCA** and PEG-thiol macromers were dyed with red and blue dyes, respectively. They were each cut in half and opposite sides were manually placed together. After one minute, the hydrogel reformed across the cut into a continuous material, as demonstrated by the final image that shows the hydrogel stretching when pulled by forceps.

Furthermore, the frequency-dependent shear moduli demonstrated excellent agreement for the pre-cut and post-cut **PEG-CBCA** hydrogel (Figure 5B) and the **PEG-BCA** hydrogel (Figure S19). In addition, exposure to repeated high and low strain (1000% and 0.5%, respectively) oscillation tests further demonstrated the self-healing behavior for the **PEG-CBCA** hydrogel (Figure 5C). Under regions of high strain (unshaded regions), the hydrogel demonstrated a decrease in storage modulus, indicating tearing or rupturing. Subsequent low-strain regions (shaded regions) allowed for the hydrogel to self-heal, as indicated by the recovery of the storage modulus. Multiple trials demonstrated the repeatability of this self-healing behavior and suggest utility for these materials in applications involving high strain such as 3D printing.

CONCLUSIONS

We have demonstrated that reversible thia-conjugate addition offers a highly tunable avenue for hydrogels crosslinked with reversible covalent bonds. The progressive synthesis of the PEG macromer enabled easy access to benzylcyanoacetamides with various aromatic substituents, which allowed for a modular synthesis that increases accessibility to a tunable range of molecular kinetics. In this work, we focused on a strong electron-withdrawing group (nitrile, **PEG-CBCA**) and a neutral directing group (hydrogen, **PEG-BCA**) to probe the effect of bond exchange kinetics on hydrogel properties. As hypothesized, the strongly electron-withdrawing group led to faster kinetics in both the forward and reverse directions. More impactful, however, was that the forward rate constant increased by a factor of nearly 20, whereas the reverse rate only increased by a factor of approximately six. When comparing the viscoelasticity of the two resulting hydrogels, those containing **PEG-CBCA** demonstrated a markedly higher plateau modulus, whereas the stress relaxation characteristics were more similar between the two hydrogels. The strong electron-withdrawing groups at the α and β sites of the unsaturated carbonyl, along with the protic aqueous environment, helped facilitate the physiologically relevant reversibility of this crosslinking system. These findings may extend beyond hydrogels to other covalent adaptable networks in which reversibility with thiol-Michael linkages currently requires elevated temperature; however, further research is required. Overall, these results demonstrate that tuning the individual kinetic rate constants for the reversible crosslinks in a polymer network enable decoupling of the resulting material mechanics. The additional kinetic control outlined in this work will enable the design of hydrogels with highly tailored moduli, stress relaxation, and self-healing behavior for applications in which dynamic properties are important.

ASSOCIATED CONTENT

Supporting Information

The Supporting Information is available free of charge at https://pubs.acs.org/doi/10.1021/acs.macromol.0c00335.

^{1}H NMR spectra, UV/vis absorbance data, reactant and product extinction coefficient data, hydrolysis data for the PEG precursors, kinetic model calculations, control experiments, and theoretical crosslinking density calculations (PDF)

AUTHOR INFORMATION

Corresponding Author

Adrianne M. Rosales − *McKetta Department of Chemical Engineering, University of Texas at Austin, Austin, Texas 78712-1589, United States;* orcid.org/0000-0003-0207-7661; Email: arosales@che.utexas.edu

https://dx.doi.org/10.1021/acs.macromol.0c00335
Macromolecules 2020, 53, 3738−3746

Authors

Thomas M. FitzSimons − *McKetta Department of Chemical Engineering, University of Texas at Austin, Austin, Texas 78712-1589, United States;* orcid.org/0000-0001-7316-475X

Felicia Oentoro − *McKetta Department of Chemical Engineering, University of Texas at Austin, Austin, Texas 78712-1589, United States*

Tej V. Shanbhag − *McKetta Department of Chemical Engineering, University of Texas at Austin, Austin, Texas 78712-1589, United States*

Eric V. Anslyn − *Department of Chemistry, University of Texas at Austin, Austin, Texas 78712-1224, United States;* orcid.org/0000-0002-5137-8797

Complete contact information is available at: https://pubs.acs.org/10.1021/acs.macromol.0c00335

Notes

The authors declare no competing financial interest.

■ ACKNOWLEDGMENTS

This research was supported by the National Science Foundation (NSF MRSEC DMR-1720595, T.M.F., E.V.A., and A.M.R.) and by the Burroughs Wellcome Fund (CASI-1015895, A.M.R.). The authors acknowledge the use of shared research facilities supported in part by the Texas Materials Institute, the Center for Dynamics and Control of Materials: an NSF MRSEC (DMR-1720595), and the NSF National Nanotechnology Coordinated Infrastructure (ECCS-1542159).

■ REFERENCES

(1) Chaudhuri, O.; Gu, L.; Klumpers, D.; Darnell, M.; Bencherif, S. A.; Weaver, J. C.; Huebsch, N.; Lee, H.-p.; Lippens, E.; Duda, G. N. Hydrogels with Tunable Stress Relaxation Regulate Stem Cell Fate and Activity. *Nat. Mater.* **2016**, *15*, 326−334.

(2) Purcell, B. P.; Lobb, D.; Charati, M. B.; Dorsey, S. M.; Wade, R. J.; Zellars, K. N.; Doviak, H.; Pettaway, S.; Logdon, C. B.; Shuman, J. A. Injectable and Bioresponsive Hydrogels for On-Demand Matrix Metalloproteinase Inhibition. *Nat. Mater.* **2014**, *13*, 653−661.

(3) Rosales, A. M.; Anseth, K. S. The Design of Reversible Hydrogels to Capture Extracellular Matrix Dynamics. *Nat. Rev. Mater.* **2016**, *1*, 1−15.

(4) Tang, S.; Ma, H.; Tu, H.-C.; Wang, H.-R.; Lin, P.-C.; Anseth, K. S. Adaptable Fast Relaxing Boronate-Based Hydrogels for Probing Cell-Matrix Interactions. *Adv. Sci.* **2018**, *5*, 1800638.

(5) Wang, H.; Heilshorn, S. C. Adaptable Hydrogel Networks with Reversible Linkages for Tissue Engineering. *Adv. Mater.* **2015**, *27*, 3717−3736.

(6) Loebel, C.; Rodell, C. B.; Chen, M. H.; Burdick, J. A. Shear-Thinning and Self-Healing Hydrogels as Injectable Therapeutics and for 3D-Printing. *Nat. Protoc.* **2017**, *12*, 1521−1541.

(7) Webber, M. J.; Appel, E. A.; Meijer, E. W.; Langer, R. Supramolecular Biomaterials. *Nat. Mater.* **2015**, *15*, 13−26.

(8) McKinnon, D. D.; Domaille, D. W.; Brown, T. E.; Kyburz, K. A.; Kiyotake, E.; Cha, J. N.; Anseth, K. S. Measuring Cellular Forces Using Bis-Aliphatic Hydrazone Crosslinked Stress-Relaxing Hydrogels. *Soft Matter* **2014**, *10*, 9230−9236.

(9) Kloxin, C. J.; Bowman, C. N. Covalent Adaptable Networks: Smart, Reconfigurable and Responsive Network Systems. *Chem. Soc. Rev.* **2013**, *42*, 7161−7173.

(10) Lou, J.; Stowers, R.; Nam, S.; Xia, Y.; Chaudhuri, O. Stress relaxing hyaluronic acid-collagen hydrogels promote cell spreading, fiber remodeling, and focal adhesion formation in 3D cell culture. *Biomaterials* **2018**, *154*, 213−222.

(11) Deng, C. C.; Brooks, W. L. A.; Abboud, K. A.; Sumerlin, B. S. Boronic Acid-Based Hydrogels Undergo Self-Healing at Neutral and Acidic PH. *ACS Macro Lett.* **2015**, *4*, 220−224.

(12) Tseng, T.-C.; Tao, L.; Hsieh, F.-Y.; Wei, Y.; Chiu, I.-M.; Hsu, S.-h. An Injectable, Self-Healing Hydrogel to Repair the Central Nervous System. *Adv. Mater.* **2015**, *27*, 3518−3524.

(13) Zhao, X.; Wu, H.; Guo, B.; Dong, R.; Qiu, Y.; Ma, P. X. Antibacterial anti-oxidant electroactive injectable hydrogel as self-healing wound dressing with hemostasis and adhesiveness for cutaneous wound healing. *Biomaterials* **2017**, *122*, 34−47.

(14) Wei, Z.; Yang, J. H.; Du, X. J.; Xu, F.; Zrinyi, M.; Osada, Y.; Li, F.; Chen, Y. M. Dextran-Based Self-Healing Hydrogels Formed by Reversible Diels-Alder Reaction under Physiological Conditions. *Macromol. Rapid Commun.* **2013**, *34*, 1464−1470.

(15) Rodell, C. B.; MacArthur, J. W.; Dorsey, S. M.; Wade, R. J.; Wang, L. L.; Woo, Y. J.; Burdick, J. A. Shear-Thinning Supramolecular Hydrogels with Secondary Autonomous Covalent Crosslinking to Modulate Viscoelastic Properties In Vivo. *Adv. Funct. Mater.* **2015**, *25*, 636−644.

(16) Yesilyurt, V.; Webber, M. J.; Appel, E. A.; Godwin, C.; Langer, R.; Anderson, D. G. Injectable Self-Healing Glucose-Responsive Hydrogels with PH-Regulated Mechanical Properties. *Adv. Mater.* **2016**, *28*, 86−91.

(17) Wang, H.; Zhu, D.; Paul, A.; Cai, L.; Enejder, A.; Yang, F.; Heilshorn, S. C. Covalently Adaptable Elastin-Like Protein-Hyaluronic Acid (ELP-HA) Hybrid Hydrogels with Secondary Thermoresponsive Crosslinking for Injectable Stem Cell Delivery. *Adv. Funct. Mater.* **2017**, *27*, 1605609.

(18) Grindy, S. C.; Learsch, R.; Mozhdehi, D.; Cheng, J.; Barrett, D. G.; Guan, Z.; Messersmith, P. B.; Holten-Andersen, N. Control of Hierarchical Polymer Mechanics with Bioinspired Metal-Coordination Dynamics. *Nat. Mater.* **2015**, *14*, 1210−1216.

(19) Fadeev, M.; Davidson-rozenfeld, G.; Biniuri, Y.; Yakobi, R.; Cazelles, R.; Aleman-garcia, M. A.; Willner, I. Redox-Triggered Hydrogels Revealing Switchable Stiffness Properties and Shape-Memory Functions. *Polym. Chem.* **2018**, *9*, 2905−2912.

(20) Tang, S.; Glassman, M. J.; Li, S.; Socrate, S.; Olsen, B. D. Oxidatively Responsive Chain Extension to Entangle Engineered Protein Hydrogels. *Macromolecules* **2014**, *47*, 791−799.

(21) Cui, J.; del Campo, A. Multivalent H-Bonds for Self-Healing Hydrogels. *Chem. Commun.* **2012**, *48*, 9302−9304.

(22) Guo, M.; Pitet, L. M.; Wyss, H. M.; Vos, M.; Dankers, P. Y. W.; Meijer, E. W. Tough Stimuli-Responsive Supramolecular Hydrogels with Hydrogen-Bonding Network Junctions. *J. Am. Chem. Soc.* **2014**, *136*, 6969−6977.

(23) Dankers, P. Y. W.; Hermans, T. M.; Baughman, T. W.; Kamikawa, Y.; Kieltyka, R. E.; Bastings, M. M. C.; Janssen, H. M.; Sommerdijk, N. A. J. M.; Larsen, A.; Van Luyn, M. J. A. Hierarchical Formation of Supramolecular Transient Networks in Water: A Modular Injectable Delivery System. *Adv. Mater.* **2012**, *24*, 2703−2709.

(24) Zhang, G.; Chen, Y.; Deng, Y.; Ngai, T.; Wang, C. Dynamic Supramolecular Hydrogels: Regulating Hydrogel Properties through Self-Complementary Quadruple Hydrogen Bonds and Thermo-Switch. *ACS Macro Lett.* **2017**, *6*, 641−646.

(25) Rodell, C. B.; Mealy, J. E.; Burdick, J. A. Supramolecular Guest-Host Interactions for the Preparation of Biomedical Materials. *Bioconjugate Chem.* **2015**, *26*, 2279−2289.

(26) Appel, E. A.; Biedermann, F.; Hoogland, D.; Del Barrio, J.; Driscoll, M. D.; Hay, S.; Wales, D. J.; Scherman, O. A. Decoupled Associative and Dissociative Processes in Strong yet Highly Dynamic Host-Guest Complexes. *J. Am. Chem. Soc.* **2017**, *139*, 12985−12993.

(27) Zou, L.; Braegelman, A. S.; Webber, M. J. Dynamic Supramolecular Hydrogels Spanning an Unprecedented Range of Host-Guest Affinity. *ACS Appl. Mater. Interfaces* **2019**, *11*, 5695−5700.

(28) Jin, Y.; Yu, C.; Denman, R. J.; Zhang, W. Recent Advances in Dynamic Covalent Chemistry. *Chem. Soc. Rev.* **2013**, *42*, 6634−6654.

(29) Cromwell, O. R.; Chung, J.; Guan, Z. Malleable and Self-Healing Covalent Polymer Networks through Tunable Dynamic Boronic Ester Bonds. *J. Am. Chem. Soc.* **2015**, *137*, 6492−6495.
(30) Boehnke, N.; Cam, C.; Bat, E.; Segura, T.; Maynard, H. D. Imine Hydrogels with Tunable Degradability for Tissue Engineering. *Biomacromolecules* **2015**, *16*, 2101−2108.
(31) McKinnon, D. D.; Domaille, D. W.; Cha, J. N.; Anseth, K. S. Bis-Aliphatic Hydrazone-Linked Hydrogels Form Most Rapidly at Physiological PH: Identifying the Origin of Hydrogel Properties with Small Molecule Kinetic Studies. *Chem. Mater.* **2014**, *26*, 2382−2387.
(32) Ghobril, C.; Charoen, K.; Rodriguez, E. K.; Nazarian, A.; Grinstaff, M. W. A Dendritic Thioester Hydrogel Based on Thiol-Thioester Exchange as a Dissolvable Sealant System for Wound Closure. *Angew. Chem., Int. Ed.* **2013**, *52*, 14070−14074.
(33) McKinnon, D. D.; Domaille, D. W.; Cha, J. N.; Anseth, K. S. Biophysically Defined and Cytocompatible Covalently Adaptable Networks as Viscoelastic 3d Cell Culture Systems. *Adv. Mater.* **2014**, *26*, 865−872.
(34) Koivusalo, L.; Karvinen, J.; Sorsa, E.; Jönkkäri, I.; Väliaho, J.; Kallio, P.; Ilmarinen, T.; Miettinen, S.; Skottman, H.; Kellomäki, M. Hydrazone Crosslinked Hyaluronan-Based Hydrogels for Therapeutic Delivery of Adipose Stem Cells to Treat Corneal Defects. *Mater. Sci. Eng., C* **2018**, *85*, 68−78.
(35) Smithmyer, M. E.; Deng, C. C.; Cassel, S. E.; Levalley, P. J.; Sumerlin, B. S.; Kloxin, A. M. Self-Healing Boronic Acid-Based Hydrogels for 3D Co-Cultures. *ACS Macro Lett.* **2018**, *7*, 1105−1110.
(36) Marco-Dufort, B.; Tibbitt, M. W. Design of Moldable Hydrogels for Biomedical Applications Using Dynamic Covalent Boronic Esters. *Mater. Today Chem.* **2019**, *12*, 16−33.
(37) Jansen, L. E.; Negrón-Piñeiro, L. J.; Galarza, S.; Peyton, S. R. Control of Thiol-Maleimide Reaction Kinetics in PEG Hydrogel Networks. *Acta Biomater.* **2018**, *70*, 120−128.
(38) Yesilyurt, V.; Ayoob, A. M.; Appel, E. A.; Borenstein, J. T.; Langer, R.; Anderson, D. G. Mixed Reversible Covalent Crosslink Kinetics Enable Precise, Hierarchical Mechanical Tuning of Hydrogel Networks. *Adv. Mater.* **2017**, *29*, 1605947.
(39) Lou, J.; Liu, F.; Lindsay, C. D.; Chaudhuri, O.; Heilshorn, S. C.; Xia, Y. Dynamic Hyaluronan Hydrogels with Temporally Modulated High Injectability and Stability Using a Biocompatible Catalyst. *Adv. Mater.* **2018**, *30*, 1705215.
(40) Accardo, J. V.; Kalow, J. A. Reversibly Tuning Hydrogel Stiffness through Photocontrolled Dynamic Covalent Crosslinks. *Chem. Sci.* **2018**, *9*, 5987−5993.
(41) Fairbanks, B. D.; Schwartz, M. P.; Halevi, A. E.; Nuttelman, C. R.; Bowman, C. N.; Anseth, K. S. A Versatile Synthetic Extracellular Matrix Mimic via Thiol-Norbornene Photopolymerization. *Adv. Mater.* **2009**, *21*, 5005−5010.
(42) Kharkar, P. M.; Kiick, K. L.; Kloxin, A. M. Design of Thiol- and Light-Sensitive Degradable Hydrogels Using Michael-Type Addition Reactions. *Polym. Chem.* **2015**, *6*, 5565−5574.
(43) Hiemstra, C.; van der Aa, L. J.; Zhong, Z.; Dijkstra, P. J.; Feijen, J. Rapidly in Situ-Forming Degradable Hydrogels from Dextran Thiols through Michael Addition. *Biomacromolecules* **2007**, *8*, 1548−1556.
(44) Hiemstra, C.; Van Der Aa, L. J.; Zhong, Z.; Dijkstra, P. J.; Feijen, J. Novel in Situ Forming, Degradable Dextran Hydrogels by Michael Addition Chemistry: Synthesis, Rheology, and Degradation. *Macromolecules* **2007**, *40*, 1165−1173.
(45) Nair, D. P.; Podgórski, M.; Chatani, S.; Gong, T.; Xi, W.; Fenoli, C. R.; Bowman, C. N. The Thiol-Michael Addition Click Reaction: A Powerful and Widely Used Tool in Materials Chemistry. *Chem. Mater.* **2013**, *26*, 724−744.
(46) Allen, C. F. H.; Happ, G. P. The Thermal Reversibility of the Michael Reaction: I. Nitriles. *Can. J. Chem.* **1964**, *42*, 641−649.
(47) Allen, C. F. H.; Humphlett, W. J. The Thermal Reversibility of the Michael Reaction: V. the Effect of the Structure of Certain Thiol Adducts on Cleavage. *Can. J. Chem.* **1966**, *44*, 2315−2321.
(48) Zhang, B.; Chakma, P.; Shulman, M. P.; Ke, J.; Digby, Z. A.; Konkolewicz, D. Probing the Mechanism of Thermally Driven Thiol-Michael Dynamic Covalent Chemistry. *Org. Biomol. Chem.* **2018**, *16*, 2725−2734.
(49) Van Herck, N.; Maes, D.; Unal, K.; Guerre, M.; Winne, J. M.; Du Prez, F. E. Covalent Adaptable Networks with Tunable Exchange Rates Based on Reversible Thiol-yne Cross-Linking. *Angew. Chem., Int. Ed.* **2020**, *59*, 3609−3617.
(50) Chakma, P.; Rodrigues Possarle, L. H.; Digby, Z. A.; Zhang, B.; Sparks, J. L.; Konkolewicz, D. Dual Stimuli Responsive Self-Healing and Malleable Materials Based on Dynamic Thiol-Michael Chemistry. *Polym. Chem.* **2017**, *8*, 6534−6543.
(51) Zhang, B.; Digby, Z. A.; Flum, J. A.; Chakma, P.; Saul, J. M.; Sparks, J. L.; Konkolewicz, D. Dynamic Thiol-Michael Chemistry for Thermoresponsive Rehealable and Malleable Networks. *Macromolecules* **2016**, *49*, 6871−6878.
(52) Daymon, S. P.; Miller, K. M. Probing the Dynamic and Rehealing Behavior of Crosslinked Polyester Networks Containing Thermoreversible Thiol-Michael Bonds. *Polymer* **2018**, *145*, 286−293.
(53) Shi, B.; Greaney, M. F. Reversible Michael Addition of Thiols as a New Tool for Dynamic Combinatorial Chemistry. *Chem. Commun.* **2005**, 886−888.
(54) Krenske, E. H.; Petter, R. C.; Houk, K. N. Kinetics and Thermodynamics of Reversible Thiol Additions to Mono- and Diactivated Michael Acceptors: Implications for the Design of Drugs That Bind Covalently to Cysteines. *J. Org. Chem.* **2016**, *81*, 11726−11733.
(55) Zhong, Y.; Xu, Y.; Anslyn, E. V. Studies of Reversible Conjugate Additions. *Eur. J. Org. Chem.* **2013**, 5017−5021.
(56) Kuhl, N.; Geitner, R.; Bose, R. K.; Bode, S.; Dietzek, B.; Schmitt, M.; Popp, J.; Garcia, S. J.; van der Zwaag, S.; Schubert, U. S. Self-Healing Polymer Networks Based on Reversible Michael Addition Reactions. *Macromol. Chem. Phys.* **2016**, *217*, 2541−2550.
(57) Kuhl, N.; Geitner, R.; Vitz, J.; Bode, S.; Schmitt, M.; Popp, J.; Schubert, U. S.; Hager, M. D. Increased Stability in Self-Healing Polymer Networks Based on Reversible Michael Addition Reactions. *J. Appl. Polym. Sci.* **2017**, *134*, 44805.
(58) Herbert, K. M.; Getty, P. T.; Dolinski, N. D.; Hertzog, J. E.; de Jong, D.; Lettow, J. H.; Romulus, J.; Onorato, J. W.; Foster, E. M.; Rowan, S. J. Dynamic reaction-induced phase separation in tunable, adaptive covalent networks. *Chem. Sci.* **2020**, Advance Article, DOI: 10.1039/D0SC00605J
(59) Parada, G. A.; Zhao, X. Ideal Reversible Polymer Networks. *Soft Matter* **2018**, *14*, 5186−5196.
(60) Sheridan, R. J.; Bowman, C. N. A Simple Relationship Relating Linear Viscoelastic Properties and Chemical Structure in a Model Diels-Alder Polymer Network. *Macromolecules* **2012**, *45*, 7634−7641.